16th World Conference on Earthquake Engineering, 16WCEE 2017
Santiago Chile, January 9th to 13th 2017
Paper N° 2963
Registration Code: S-X1463158537

COLLAPSE ASSESSMENT OF CONTROLLED ROCKING STEEL BRACED FRAMES WITH DIFFERENT ROCKING JOINT PARAMETERS

T. C. Steele(1), L. D. A. Wiebe(2)

(1) Ph.D. Candidate, Department of Civil Engineering, McMaster University, Canada, steeletc@mcmaster.ca
(2) Assistant Professor, Department of Civil Engineering, McMaster University, Canada, wiebel@mcmaster.ca

Abstract

Previous studies have shown that designing controlled rocking steel braced frames (CRSBFs) using a response modification factor of R = 8 is sufficient to prevent collapse of structures during earthquakes higher than the design level. However, it has also been suggested that CRSBFs could be designed using higher response modification factors (R), and that additional rocking joints could be used to mitigate higher mode force demands. This paper examines how the selection of R and the specification of additional rocking joints above the base influence the collapse risk of CRSBFs, as assessed using incremental dynamic analysis (IDA) and the FEMA P695 methodology. Six designs are considered, in which different base rocking joints are designed for one six-storey frame using different R values and post-tensioning arrangements. An additional six scenarios are considered, in which the same base rocking joints are used in combination with a second rocking joint above the second storey. A suite of 44 ground motions is selected and scaled until collapse occurs in at least 50% of the cases, and collapse fragility functions are generated using the truncated IDA curves. In all twelve cases, the probability of collapse is less than 10% during a 2% in 50 year event. However, the results show that R and the post-tensioning arrangement have a large influence on the collapse risk, while adding rocking joints above the base has a less significant influence.

Keywords: controlled rocking steel braced frames, self-centering systems, higher mode mitigation, incremental dynamic analysis, collapse risk assessment

1. Introduction

Controlled rocking steel braced frames (CRSBFs) are high-performance self-centering lateral force resisting systems that can be designed to mitigate structural damage during earthquakes larger than the design level [1, 2, 3, 4]. Prestressed vertical post-tensioning strands and the frame self-weight provide the restoring force to self-center the system after rocking, and energy dissipation may be provided to reduce the peak displacement demands. Additional mechanisms, such as upper rocking joints, can be added to the frame to limit the force demand on the frame members from the higher mode response [5]. As shown in Fig. 1, CRSBFs are designed to exhibit a characteristic flag-shaped hysteresis while they respond within their self-centering range during design-level earthquakes, thus allowing CRSBFs to limit structural damage and residual drifts. Several parametric studies have been performed on self-centering systems using single-degree-of-freedom (SDOF) analyses with the flag-shaped hysteresis to evaluate the ability of systems like CRSBFs to meet displacement limits during design-level earthquakes [6, 7, 8, 9]. The effects of parameters such as the response modification factor, R, nonlinear stiffness, αk, and hysteretic damping coefficient, β, on the displacements in self-centering systems have been accounted for during these studies. However, while these analyses have provided insight as to the displacements in self-centering systems that remain within the self-centering range, the flag-shaped hysteresis used in these studies did not exhibit the behavior of real structures leading up to collapse, such as damage and strength degradation of components, and therefore these studies have not assessed the collapse limits of self-centering systems such as CRSBFs. In addition, the use of higher-mode mitigation mechanisms in the design of CRSBFs cannot be evaluated using SDOF analyses.

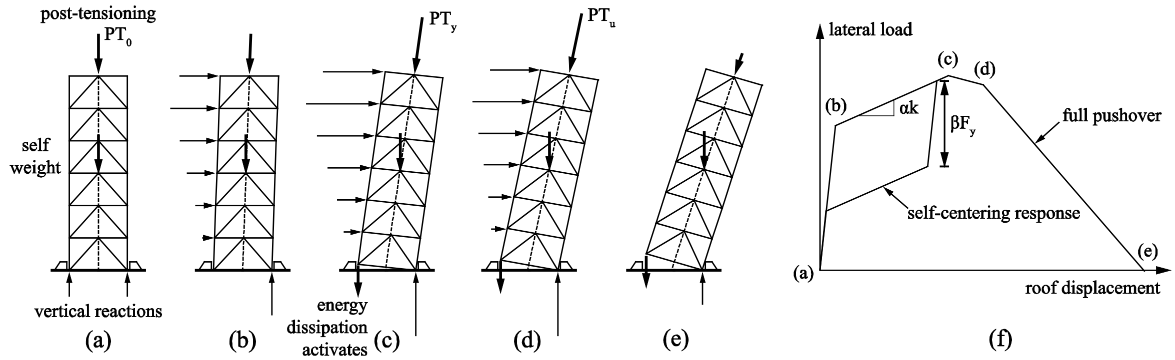

Fig. 1 – Sidesway collapse mechanism of controlled rocking steel braced frame post-tensioned with high-strength steel strands; a) initial equilibrium, b) incipient rocking, c) strand yielding, d) initial wire facture and loss of prestress, e) loss of strand stiffness and collapse, f) backbone curve

In CRSBFs, the flag-shaped hysteretic response is controlled by the selection and positioning of the post-tensioning and energy dissipating components, referred to in this paper as the design of the base rocking joint. This makes the nonlinear response of CRSBFs unique from that of other ductile structures in that the designers have a great amount of control over the seismic design parameters, including the overstrength, displacement capacity, nonlinear stiffness, and hysteretic damping, even before selecting the frame member sizes. The design of CRSBFs generally begins with the design of the base rocking joint, where the post-tensioning and energy dissipation components are designed to limit the peak displacements and to provide sufficient margins against sidesway collapse from over-rotation of the CRSBF. Past research included studies where the researchers performed collapse assessments on CRSBFs [3, 10], which have shown that CRSBFs can provide adequate collapse prevention characteristics for the designs that were considered. However, those studies were limited to structures with rocking only at the base, for a specific set of base rocking joint design parameters; different designs for the same structure may have very different collapse performance characteristics.

This paper focuses on the collapse performance of CRSBFs in which collapse is governed by failure of the base rocking joint, and presents the results of twelve incremental dynamic analyses and the corresponding collapse fragility curves for a six-storey structure with CRSBFs as the lateral force resisting system. The structure was designed for a site of high seismicity using a variety of different parameters for a total of twelve different base rocking joint designs. Six design scenarios are considered, in which the response modification factor, R, and post-tensioning arrangement are varied to evaluate the influence of these parameters on the collapse performance of the structure. Six additional design scenarios are considered, in which the same base rocking joints are used in combination with a second rocking joint at the second storey to evaluate the influence of including additional rocking joints as a higher-mode force mitigation mechanism on the collapse performance of mid-rise CRSBFs. The twelve design scenarios for this six-storey building are then subjected to a suite of 44 ground motions, which are scaled using incremental dynamic analysis to generate collapse fragility functions and determine the collapse intensity for each structure.

2. Design of the Prototype Controlled Rocking Steel Braced Frames

The study presented in this paper uses a six-storey example CRSBF with six different base rocking joints, all designed for a site of high seismicity in the western United States with short period spectral acceleration of $S_S = 1.5$ g, one second period spectral acceleration of $S_1 = 0.6$ g, and a long-period transition period of $T_L = 12$ s. The site is seismic Class D as defined in ASCE 7-10 ($V_{s,30} = 259$ m/s), with short- and long-period site coefficients of $F_a = 1.0$ and $F_v = 1.5$, respectively [11]. Fig. 2(a) displays the 10% in 50 year and the doubled 2% in 50 year elastic design spectra used to design the CRSBFs. Fig. 2(b) shows the floor plan for the example structure, which had equal storey heights of 4.57 m, and a total seismic weight of 10 200 kN and 6430 kN for each floor and the roof, respectively. The site is located in an area with a basic wind velocity of 51 m/s and wind exposure category Class B [11].

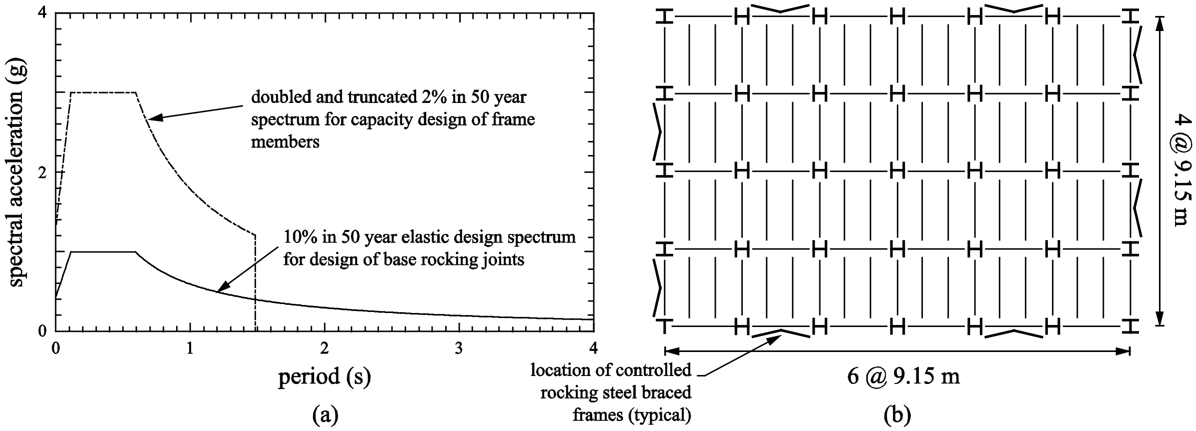

Fig. 2 – Elastic design spectra and floor plan for design of the base rocking joint and the frame members

The structure was designed according to the methodology of Wiebe and Christopoulos [4], in which the design of controlled rocking steel braced frames (CRSBFs) is separated into two main steps. First, the base rocking joint is designed for the structure to meet targeted displacement limits at different hazard levels and to provide acceptable safety against collapse due to over-rotation of the CRSBF. Second, the frame members and connections are designed to prevent yielding and buckling during events larger than the design level. The following subsections describe these two steps in detail.

2.1 Design of the base rocking joints

The base rocking joints were designed with four frames to resist the seismic demand in each direction. The frames were assumed to have specific floor-to-frame connection detailing that allows the members of the CRSBFs to be designed to not carry any gravity loads; rather, the frames were designed to be 8.23 m wide to fit between the gravity columns at each end of the 9.15 m wide bays. The design base shear for the building was calculated using the modelled first-mode period and was distributed along the height of the building using the equivalent lateral force procedure in accordance with ASCE 7-10 [10]. While a response modification factor of R = 8 has been recommended for the design of the base rocking joint in CRSBFs by several researchers [1, 2, 10], others have suggested that displacement limits for design level earthquakes could still be met while using larger response modification factors [6, 9]. However, the use of response modification factors greater than R = 8 to design CRSBFs has not been supported by any collapse risk assessment, and the use of R = 8 has only been supported by a limited collapse assessment for selected designs [3, 10]. Wiebe and Christopoulos [6] suggested that self-centering systems with first-mode periods of 0.6 s or larger may have acceptable seismic performance even if designed with response modification factors of up to R = 100, but that overturning due to wind loads or other practical constraints may limit the magnitude of the response modification factor. For the six-storey structure considered in this study, wind loads limited the overturning resistance of the CRSBF to have an effective response modification factor of R = 30. Therefore, R = 8, R = 20, and R = 30 were used to design the base rocking joints.

Table 1 displays the base rocking joint parameters for each of the six base rocking designs. The base rocking joints were designed to resist the overturning moment resulting from the equivalent lateral forces using recommendations made by Wiebe and Christopoulos [7] and Steele and Wiebe [13] to proportion the energy dissipation and post-tensioning components. The energy dissipation ratio, β (defined in Fig. 1(f) as the ratio of the height of the flag to the linear limit), was selected to be 0.8, and post-tensioning prestress ratio (defined as the ratio of the prestress to the ultimate stress) was selected to be 0.25, to ensure the post-tensioning remains elastic for normalised roof displacements of at least 2.0%, and to provide a positive post-uplift stiffness. As shown in Fig. 3, for each response modification factor used, two cases were considered where the post-tensioning was placed at either the centre at the top of the frame (PTI), or at the edges of the frame on top of the columns (PTII); the frames were also considered with rocking only at the base (1RJ) and with rocking at both the base and at the second storey (2RJ). The post-tensioning strands are continuous between the base of the frame

Table 1 – Base rocking joint design parameters

Base Rocking Joint	R	β	η	δ_{target}	ED_{act} [a]	$N_{s,PT}$	Ω [c]
R8-PTI	8	0.8	0.25	4.13%	1370 kN	59	2.68
R8-PTII	8	0.8	0.25	2.07%	1370 kN	30+30 [b]	2.72
R20-PTI	20	0.8	0.25	4.13%	550 kN	24	2.72
R20-PTII	20	0.8	0.25	2.07%	550 kN	12+12 [b]	2.72
R30-PTI	30	0.8	0.25	4.13%	370 kN	16	2.73
R30-PTII	30	0.8	0.25	2.07%	370 kN	8+8 [b]	2.73

[a] Energy dissipation activation forces equal for upper and lower rocking joints in 2RJ design cases
[b] Half of total post-tensioning anchored on top of each column
[c] Overstrength calculated using undeformed geometry

and the anchored location at the top of the frame. The normalised roof displacement before yielding of the post-tensioning was targeted assuming a rigid-rocking behaviour (i.e. the normalised roof displacement is equal to the rotation of the CRSBF) using Eq. (1):

$$\delta_{target} = (\varepsilon_{y,PT} - \varepsilon_{0,PT})\, L_{PT}/d_{PT} \geq 2.0\% \tag{1}$$

where $\varepsilon_{y,PT}$ is the post-tensioning yield strain, $\varepsilon_{0,PT}$ is initial the post-tensioning strain from the applied prestress, L_{PT} is the length of the post-tensioning strands, and d_{PT} is the distance from the rocking toe to the furthest post-tensioning strands. The target normalised roof displacement for post-tensioning yielding, the number of post-tensioning strands, $N_{s,PT}$, and the overstrength factor, Ω, for each base rocking joint design are also shown in Table 1. The second rocking joint in each frame was designed using recommendations made by Wiebe and Christopoulos [5]; the same amount of energy dissipation was specified for the upper joint as for the base rocking joint. Six designs were considered where the frame included rocking only at the base, and another six design scenarios included a second rocking joint at the second storey, for a total of 12 unique design scenarios.

2.2 Design of the capacity-protected elements

The CRSBF members were designed according to the dynamic procedure proposed by Steele and Wiebe [13] using the structural analysis program ETABS [14]. The first-mode lateral forces and corresponding ultimate post-tensioning and energy dissipation forces were used from the base rocking joint that created the largest demand on the frame members of the CRSBFs, such that the frame members would be the same for all designs, regardless of the number of rocking joints of the design of each base rocking joint. This was done to eliminate the influence of any changes to the system stiffness on the analysis results, even though a more efficient base

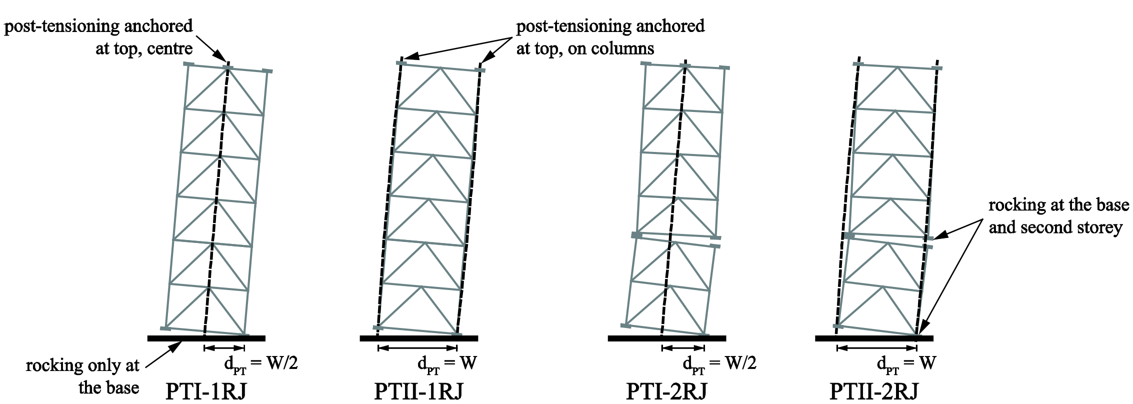

Fig. 3 – Schematic of post-tensioning arrangements and rocking joint layouts

rocking joint design or the use of the second rocking joint can also reduce the required member size. The contribution of the higher mode response to the frame member forces was estimated at twice the 2% in 50 year hazard level to provide a low probability of frame member failure during even the most extreme ground motions, since the goal of this study is to isolate failure of the base-rocking joint in the collapse assessment.

The brace-to-gusset plate connections were designed to resist the full overstrength yield force from the braces. Since this study does not include the performance of the connections in CRSBFs, only a preliminary design was completed to account for the effect of rigid offsets on the stiffness of the frame.

3. Numerical Modelling of the Prototype Frames

The six-storey frame was modelled using the earthquake engineering simulation software OpenSees [15]. Fig. 4 displays a schematic of the model for the six-storey frame used for the analyses. The frame members were all modelled using elastic elements, because the design method is assumed to provide sufficient safety against member failure during even the most extreme earthquakes. The vertical struts were all modelled as continuous, and the horizontal struts and braces were both pinned at the gusset plate connection. The energy dissipating frictional interfaces were included as truss elements using the Elastic-Perfectly plastic material model, with a yield force equal to the specified slip load. The frictional interfaces were assumed to have a maximum stroke that was sufficiently long to maintain the specified slip load up to collapse. Assuming a collapse displacement of 10%, this corresponds to a required stroke of less than 900 mm. The post-tensioning was modelled using co-rotational truss elements; yielding, initial fracture, and complete fracture of the post-tensioning strands were all simulated using the multi-linear material model suggested by Ma et al. [3], and the prestress in the post-tensioning strands was modelled by wrapping the multi-linear material in an initial stress material model. This is shown in Fig. 4(b), where the post-tensioning material model had an elastic modulus of 195 GPa, and yield, ultimate, and complete fracture strains of $\varepsilon_y = 0.83\%$, $\varepsilon_u = 1.3\%$, and $\varepsilon_{max} = 4.8\%$, which corresponded to stresses of $f_y = 1670$ MPa, $f_u = 1860$ MPa, and zero, respectively [3, 16]. Elastic buckling of the post-tensioning at negligible compressive loads was modelled using tension-only gap elements at the base of the post-tensioning.

Initial stiffness- and mass-proportional Rayleigh damping was applied to the linear elastic elements in the model assuming a damping ratio of 5% using parameters that were computed using the frequencies calculated using Eq. (2) and Eq. (3) [17]:

$$\omega_A = 1.1\omega_1/\mu^{0.5} \tag{2}$$

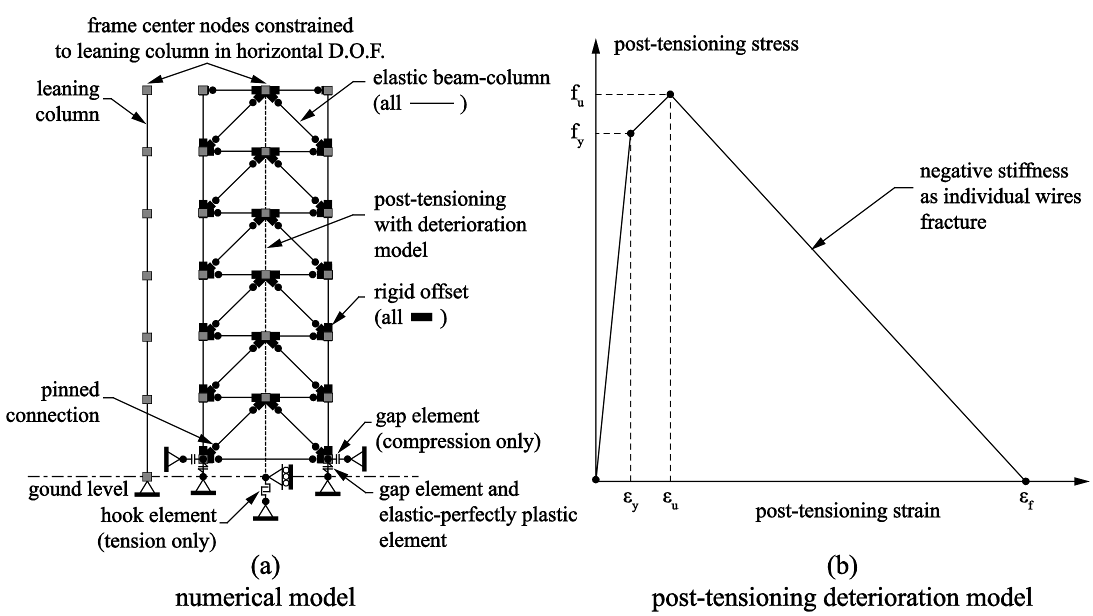

Fig. 4 – Schematic of the numerical model and post-tensioning deterioration model

$$\omega_B = 0.85\omega_1 \tag{3}$$

where ω_1 is the circular natural frequency of the first mode, and μ is the ductility of the structural system (defined in this paper as the period-based ductility used in FEMA P695 [19]). This damping model has been shown to be particularly effective for structures where the response is governed by the first mode [18]. However, the response parameters are expected to be sensitive to the assumptions made when applying the damping model.

The first-mode period was estimated to be 0.82 s using the empirical equation provided in ASCE 7-10, including the upper limit factor of 1.4 for sites where S_{D1} > 0.4 g [11]. The first-mode period from the modal analysis of the frame in OpenSees was 0.73 s, which is only 10% lower than the estimated period. However, this equation has been less accurate when estimating the fundamental periods of other example CRSBFs [5, 13].

Fig. 5 shows the pushover curves for the frame with the six different base rocking joints. The lateral strength is normalised by the linear limit of the structure (defined in Fig. 1(f) as the lateral load at which the structure begins to rock) with the base-rocking joint designed using R = 8, and plotted against the normalised lateral roof displacement (i.e. roof displacement / building height). From the pushover curves, it is shown that the post-tensioning begins to yield at roof displacements larger than the 2.07% and 4.13% normalised roof drift estimated from Eq. (1); this is because the frame has some flexibility, and because the post-tensioning compresses the frame as it extends, which means the base rotation will place slightly less strain demand on the post-tensioning than originally assumed. The six different base rocking joints led to a wide range of pushover responses under the code-prescribed first-mode lateral forces. However, the pushover curves are the same for each frame, regardless of whether an additional rocking joint is included at the second storey.

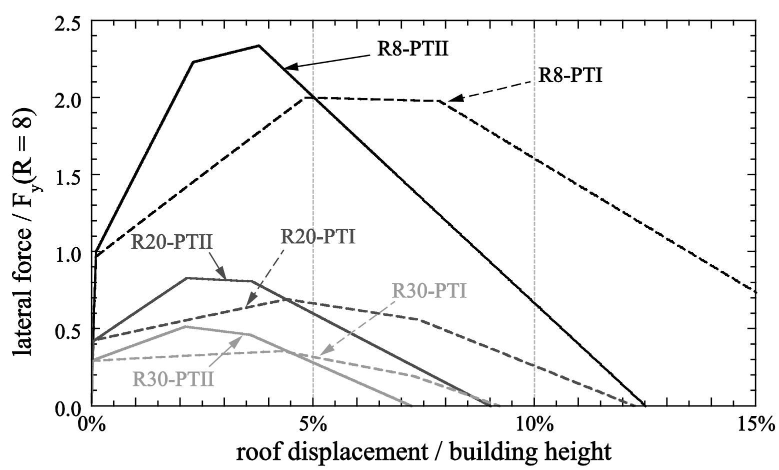

Fig. 5 – Pushover curves for the six-storey frame with the six different base rocking joint designs

4. Incremental Dynamic Analysis and Collapse Risk Assessment

Evaluating the collapse capacity of structures under seismic loading requires a suite of strong ground motions with enough records to generate sufficient data points to fit a collapse fragility curve. The FEMA P695 suite of 44 strong far-field ground motions (22 horizontal pairs), was adopted for this study [19]. The ground motions were scaled collectively to match the median of the ground motion records to the 2% in 50 year elastic design spectrum at the first-mode period of building; the resulting scaling factor was 2.48. To generate the collapse fragility curves for each base rocking joint design, incremental dynamic analysis (IDA) was performed for each of the example structures using a sequence of nonlinear time history analyses [20]. The nonlinear time history analyses were completed for each of the 44 ground motions scaled up to collapse in 10% increments relative to the 2% in 50 year intensity level using the numerical model discussed in Section 3 until at least half of the records in the suite caused collapse. The records causing collapse were scaled in more refined increments near the collapse intensity. The engineering demand parameter used to represent sidesway collapse of the CRSBFs was the peak interstorey drift, and the intensity measure was the 5% damped spectral acceleration at the first-mode period of the structures. The frame collapse intensity was defined as that which caused the interstorey drift of the structure to exceed 10%, beyond which the gravity framing was assumed to lose its ability to support the gravity loads in the structure. The collapse data points from the truncated IDA curves were used to estimate the median collapse intensity, $\hat{S}_{CT}$, and the record-to-record variability, β_{RTR}, assuming a lognormal distribution using the software tools provided by Baker [21].

Next, the median collapse intensity ($\hat{S}_{CT}$) was amplified to account for the effect of the spectral shape of the ground motions used to perform the incremental dynamic analysis, as past researchers have shown that spectral shape has a significant influence on the performance of ductile structures when they experience significant nonlinear displacements [22]. The FEMA P695 documents [19] include a simple method to estimate the influence of the spectral shape of the collapse capacity of the system through the use of a spectral shape factor (SSF). This factor was 1.41 for all of the frames in this study, and was applied to the intensity of the incremental dynamic analysis results to account for the reduction in the collapse capacity that is observed when using a generic ground motion suite such as the one recommended in FEMA P695 [19, 21].

Finally, the collapse fragility curves were generated to incorporate additional system-level uncertainty beyond the record-to-record variability. The recommendations in FEMA P695 were used in this study, where additional system-level uncertainty is added from three categories: the robustness of the design requirements, the accuracy of the test data, and the accuracy of the numerical model [19]. The total system uncertainty was calculated by combining the uncertainty parameters using Eq. (4):

$$\beta_{TOT} = [\beta_{RTR}{}^2 + \beta_{DR}{}^2 + \beta_{TD}{}^2 + \beta_{MDL}{}^2]^{0.5} \tag{4}$$

where β_{RTR} is the record-to-record variability of the collapse data, β_{DR} is the additional uncertainty associated with the robustness of the design requirements, β_{TD} is the additional uncertainty associated with the accuracy of the test data, and β_{MDL} is the additional uncertainty associated with the accuracy of the numerical model. While the record-to-record variability can be estimated from the collapse data, the other uncertainty parameters that contribute to the total system uncertainty can be subjectively ranked as “superior,” “good,” “fair,” or “poor,” which correspond to values of 0.1, 0.2, 0.35 and 0.5, respectively [19]. The design method is assumed to be sufficiently robust such that it warranted a "superior" rating (i.e. β_{DR} = 0.1). Three cases were considered where the accuracy of the test data and numerical model were both assigned the same rating of “superior,” “good,” “fair.” Using these three different ratings for the additional system-level uncertainty, three different collapse fragility curves were generated, so as to evaluate the influence of this additional uncertainty on the collapse risk associated with each design.

The FEMA P695 methodology requires that the probability of collapse during a 2% in 50 year event be less than 10% [19]. This acceptance criterion can be evaluated by calculating the adjusted collapse margin ratio (ACMR) using Eq. (5):

$$ACMR = \hat{S}_{CT}/S_{MT} \times SSF \tag{5}$$

where S_{MT} is the spectral acceleration from the 2% in 50 year elastic design spectrum at the first-mode period. The ACMR can then be compared to the acceptable value at which the collapse probability of the structure is 10% for a given total system uncertainty, as shown in Eq. (6):

$$ACMR \geq ACMR_{10\%}(\beta_{TOT}) \tag{6}$$

The ACMR is a measure of the capacity each design has against collapse. In this study, rather than comparing the ACMR to the acceptable value, the probability of collapse during a 2% in 50 year event is determined from the collapse fragility curves where $[S_a(T_1, 5\%)/S_{MT}] \times SSF = 1$ and is considered to be acceptably low if it is less than the 10% limit. Both the ACMR and the probability of collapse during a 2% in 50 year event can be taken directly from the collapse fragility curves presented in this section, because the collapse fragility curves

Table 2 – Collapse assessment results

Frame	μ_T	$\hat{S}_{CT}$	β_{RTR}	ACMR	Probability of collapse during a 2% in 50 year event (Acceptable if < 10%)		
					Superior[a]	Good[b]	Fair[c]
R8-PTI-1RJ	55.2	5.23	0.44	6.00	0.0000%	0.012%	0.288%
R8-PTII-1RJ	26.4	4.50	0.40	5.16	0.0000%	0.018%	0.431%
R20-PTI-1RJ	120	4.12	0.60	4.72	0.664%	1.05%	2.42%
R20-PTII-1RJ	62.6	2.90	0.52	3.32	1.01%	1.79%	4.36%
R30-PTI-1RJ	181	3.35	0.62	3.84	1.89%	2.60%	4.69%
R30-PTII-1RJ	84.9	2.36	0.51	2.71	3.01%	4.40%	8.09%
R8-PTI-2RJ	55.2	4.48	0.35	5.13	0.0007%	0.019%	0.384%
R8-PTII-2RJ	26.4	4.05	0.31	4.64	0.0013%	0.027%	0.467%
R20-PTI-2RJ	120	2.94	0.35	3.37	0.098%	0.433%	2.43%
R20-PTII-2RJ	62.6	2.42	0.34	2.77	0.402%	1.27%	4.75%
R30-PTI-2RJ	181	2.30	0.30	2.64	0.288%	1.18%	5.04%
R30-PTII-2RJ	84.9	1.98	0.37	2.27	2.31%	4.35%	9.61%

[a-c]Subjective ratings assigned to both test data and numerical model uncertainties

have been adjusted for the additional system-level uncertainty and spectral shape, and also normalised by the 2% in 50 year intensity [19].

4.1 Influence of response modification factor on collapse risk

Fig. 6 displays the collapse fragility curves for the six-storey frame for the different base rocking joints that were designed using force reduction factors of R = 8, R = 20, and R = 30. Table 2 shows the corresponding period-based ductility, median collapse intensity, record-to-record variability, adjusted collapse margin ratio, and the probability of collapse during a 2% in 50 year event considering the three different levels of additional system-level uncertainty. For the base rocking joint designed with the post-tensioning in the middle of the frame, increasing the response modification factor from R = 8 to R = 20 reduced the ACMR value by 21% from 6.00 to 4.72; this corresponded to an increase in the probability of collapse during a 2% in 50 year event by a factor of 8.40 from 0.288% to 2.42% when the additional system-level uncertainty was rated as "fair." For the base rocking joint designed with the post-tensioning at the edges of the frame, the same increase in the response modification factor reduced the ACMR value by 35% from 5.16 to 3.32; this corresponded to an increase in the probability of collapse during a 2% in 50 year event by a factor of 10.1 from 0.431% to 4.36% when the additional system-level uncertainty was rated as "fair." However, for both post-tensioning arrangements, using a response modification factor of R = 20 led to probabilities of collapse during a 2% in 50 year event that were less than the 10% limit, regardless of the rating assigned to the additional system-level uncertainty.

For the base rocking joint designed with the post-tensioning in the middle of the frame, increasing the response modification factor from R = 20 to R = 30 reduced the ACMR value by another 19% from 4.72 to 3.84; this corresponded to an increase in the probability of collapse during a 2% in 50 year event by a factor of 1.94 from 2.42% to 4.69% when the additional system-level uncertainty was rated as "fair." For the base rocking joint designed with the post-tensioning at the edges of the frame, the same increase in the response modification factor reduced the ACMR value by an additional 19% from 3.32 to 2.71; this corresponded to an increase in the probability of collapse during a 2% in 50 year event by a factor of 1.86 from 4.36% to 8.09% when the additional system-level uncertainty was rated as "fair." For both post-tensioning arrangements, using a response modification factor of R = 30 led to probabilities of collapse during a 2% in 50 year event that were less than the 10% limit when the additional system-level uncertainty was rated as "fair" or better. In general, increasing the response modification factor decreased the collapse capacity of the structure, and as a consequence, increased

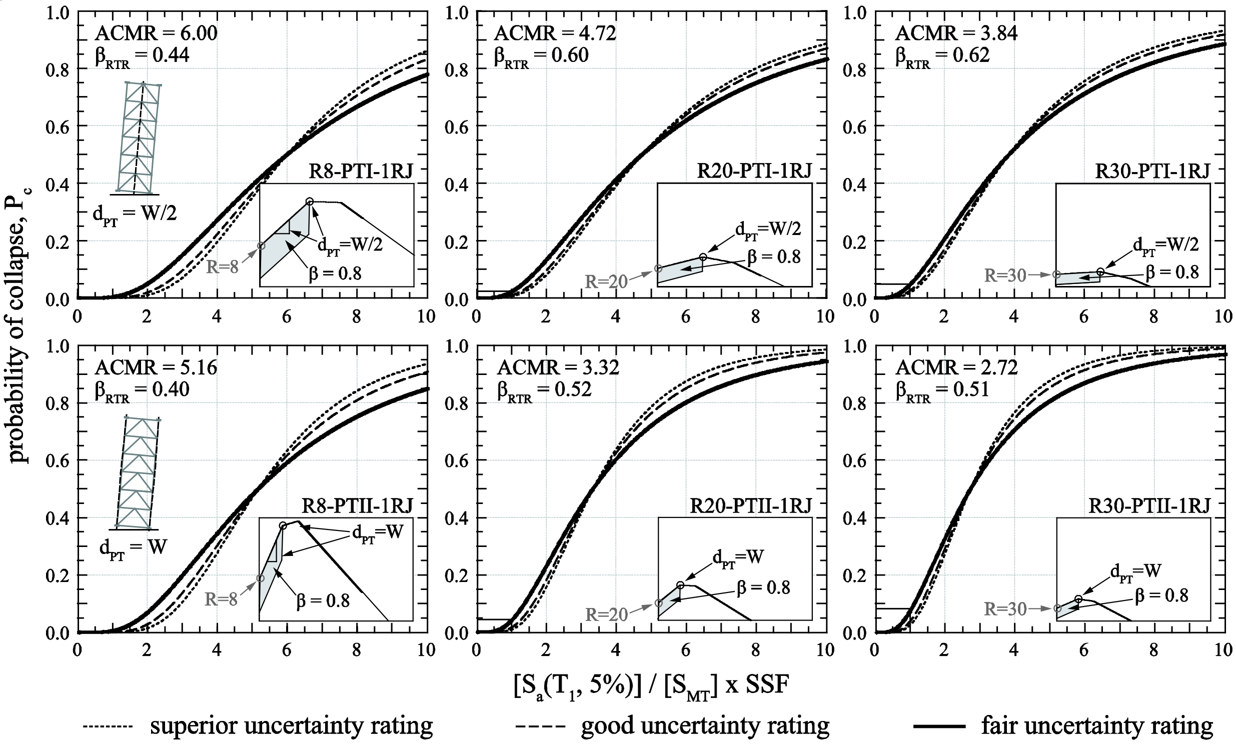

Fig. 6 – Fragility functions for the frames designed using response modification factors of 8, 20 and 30; and post-tensioning anchored at the middle or edges of the frame

the collapse risk. This was expected, as increasing the response modification factor has been shown to decrease the collapse capacity of structures in general [19]. However, the results also show that response modification factors as high at R = 30 can provide sufficient collapse capacity to mid-rise CRSBFs. However, more archetypes should be considered as described in FEMA P695 before response modification factors larger than R = 8 can be recommended for codification.

4.2 Influence of post-tensioning arrangement on collapse risk

In addition to the response modification factor, the post-tensioning arrangement was found to have a significant influence of the collapse risk in CRSBFs. Placing the post-tensioning at the edges of the frame (as opposed to at the centre of the frame) nearly doubled the probability of collapse during a 2% in 50 year event in each of the cases considered. For the base rocking joints designed using a response modification factor of R = 8, moving the post-tensioning from the centre of the frame to the edges of the frame decreased the ACMR value by 14% from 6.00 to 5.16, increasing the probability of collapse during a 2% in 50 year event by a factor of 1.5 from 0.288% to 0.431% when the additional system-level uncertainty was rated as “fair.” For the base rocking joints designed using response modification factors of R = 20 and R = 30, moving the post-tensioning from the centre of the frame to the edges of the frame decreased the ACMR values in each case by 30%, from 4.72 to 3.32 and from 3.35 to 2.36, respectively. This corresponded to increases in the probability of collapse during a 2% in 50 year event by factors of 1.80 and 1.72, from 2.42% to 4.36% and from 4.69% to 8.09%, respectively when the additional system-level uncertainty was rated as “fair.” The decrease in collapse capacity was due to the increase in the strain demands in the post-tensioning strands when they were placed at the frame edges, causing them to yield and fracture during less intense ground motions. This is also shown in the pushover curves from Fig. 5, which are overlain on the collapse fragility curves to demonstrate the difference in strength and stiffness between the post-tensioning arrangements. In each case, moving the post-tensioning outward from the center of the frame to the edges had a similar influence on the collapse capacity and risk as increasing the response modification factor from R = 20 to R = 30.

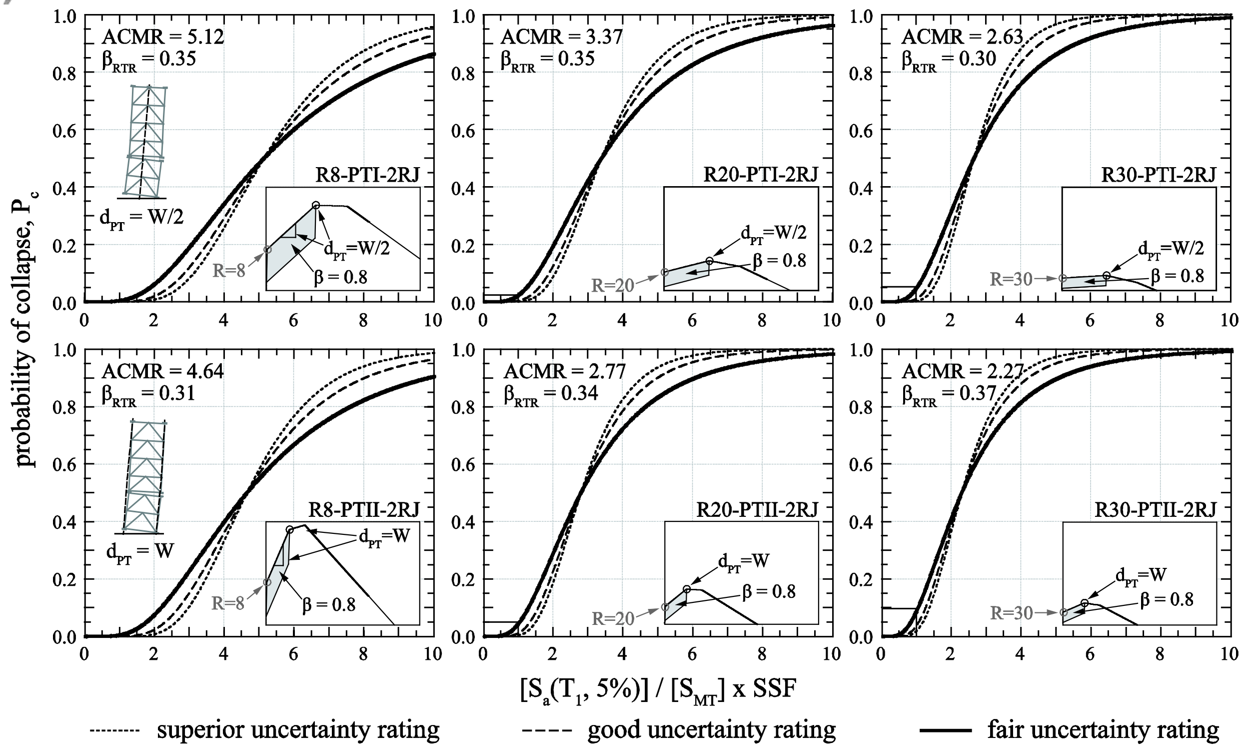

Fig. 7 – Fragility functions for the frames an additional rocking joint at the second storey

4.3 Influence of additional rocking joint on collapse risk

Fig. 7 displays the collapse fragility curves for the six-storey frame analysed using the same base rocking joints, but with an additional rocking joint at the second storey to mitigate the force demand from the higher-mode response. The addition of a second rocking joint decreased the ACMR and generally increased the probability of collapse during a 2% in 50 year event for each of the cases considered in this study. However, the addition of a second rocking joint did not have as large an influence as either increasing the response modification factor or changing the post-tensioning arrangement. Adding the second rocking joint had the largest relative influence on the base rocking joint designed using R = 8 with the post-tensioning placed in the center of the frame, where adding the second rocking joint at the second storey decreased the ACMR by 15% from 5.23 to 4.48, thereby increasing the probability of collapse during a 2% in 50 year event by 33% from 0.288% to 0.384% when the additional system-level uncertainty was rated as “fair.” The decrease in collapse capacity was due to the second rocking joint placing additional strain demand on the post-tensioning, causing it to yield and fracture during less intense ground motions. However, reducing the ACMR did not always correspond to as large an increase in the probability of collapse during a 2% in 50 year event. For the base rocking joint designed using R = 20 with the post-tensioning placed in the centre of the frame, the 29% decrease in ACMR from 4.72 to 3.37 had almost no influence on the probability of collapse during a 2% in 50 year event when the additional system-level uncertainty was rated as “fair.” This was because the record-to-record variability of the collapse intensities was decreased when the second rocking joint was added, which reduced the total system uncertainty. This decreased the dispersion of the collapse fragility curve, which decreased the probability of collapse at the 2% in 50 year intensity level.

Although the collapse capacity was reduced when a second rocking joint was added at the second storey, and this generally increased the probability of collapse, the probability of collapse during a 2% in 50 year event was still below the 10% limit as long as the additional system-level uncertainty was rated “fair” or better. Including multiple rocking joints along the height of the building has been shown to reduce the member force demands from the higher mode response [4, 9], which can allow designers to select smaller member sizes.

5. Conclusions

This study examined the influence that the response modification factor, post-tensioning arrangement, and use of higher mode mitigation mechanisms (such as additional rocking joints) have on the collapse capacity of a CRSBF. This was done based on incremental dynamic analysis of twelve designs of six-storey frames, using the data to estimate the collapse fragility curves for each design using the FEMA P695 methodology [17]. Increasing the response modification factor had the largest influence on the collapse capacity, as increasing the response modification factor from R = 8 to R = 30 increased the probability of collapse by up to sixteen times in the cases considered. However, all of the cases presented in this study limited the probability of collapse during a 2% in 50 year event to less than 10%, even when the base rocking joints were designed using response modification factors much larger than R = 8. Reducing the displacement capacity of the CRSBFs caused a noticeable reduction in the adjusted collapse margin ratio (ACMR), thereby increasing the collapse probability; this was demonstrated in this study by moving the post-tensioning strands from the center of the frame to the edges of the frame, which increases the displacement demand on the post-tensioning strands for a given base rotation. However, this can also happen if the post-tensioning prestress ratio is increased or if the length of the post-tensioning strands is decreased. The placement of the post-tensioning strands had as much of an influence on the collapse performance of the CRSBFs as changing the response modification factor from R = 20 to R = 30. Including a second rocking joint at the second storey of the six-storey CRSBFs had the least influence on the collapse capacity and collapse risk. While the additional rocking joint reduced the ACMR by up to 30%, it also decreased the uncertainty in the collapse data, leading to less significant increases in collapse risk. This could result in an overall improvement of the performance of CRSBFs, as specifying additional rocking joints as a higher mode mitigation mechanism has been shown to reduce both the force demands in the frame members and also the floor accelerations.

All of the twelve example design scenarios considered had probabilities of collapse that were less than the 10% limit during a 2% in 50 year event when the additional system-level uncertainty was rated as “fair” or better. This suggests that CRSBFs designed using a response modification factor of up to R = 30 may be able to provide safety against collapse. However, this study was limited to one six-storey structure without significant geometric, stiffness, or mass irregularities, and where the CRSBFs were designed using high-strength post-tensioning strands and frictional energy dissipating interfaces. While the relative comparisons of the different base rocking joints presented in this study are expected to be unaffected by the assumptions made, the numerical results may be sensitive to the gravity loads in the structure, the structure geometry, the behaviour of different post-tensioning tendons, and the type of energy dissipation used. In addition, the frame members were assumed to remain elastic during even the more extreme ground motions; member buckling, yielding, and deterioration were not considered in the analyses. While the design method implemented in this study was assumed to provide a significant safeguard against failure of the frame members by accounting for the higher-mode contribution to the capacity design forces at twice the 2% in 50 year hazard level, the adjusted collapse margin ratio was greater than two (as high as 6.00) for the structure for all of the twelve design scenarios. This may lead to collapse mechanisms that are governed by member failure limit states rather than over-rotation of the base rocking joint, particularly if higher mode mitigation mechanisms (e.g. including additional rocking joints above the base) are not included. Therefore, further research is ongoing to evaluate the influence of frame member failure on the collapse performance of CRSBFs.

Acknowledgements

Financial support for this research from the Natural Science and Engineering Research Council of Canada (NSERC), the Government of Ontario, the Canadian Institute of Steel Construction (CISC) and the McMaster University Faculty of Engineering is gratefully acknowledged.

References

[1] Roke D, Sause R, Ricles JM, Chancellor NB (2010): Damage-free seismic resistant self-centering concentrically braced frames. *ATLSS Report 10-09*. ATLSS Engineering Research Center, Bethlehem, PA, USA.

[2] Eatherton MR, Hajjar JF (2010): Large-scale cyclic and hybrid simulation testing and development of a controlled-rocking steel building system with replaceable fuses, *NSEL Report NSEL-025*, Department of Civil and Environmental Engineering, University of Illinois at Urbana-Champaign, Urbana, IL, USA.

[3] Ma X, Krawinkler H, Deierlein G (2011): Seismic design and behavior of self-centering braced frames with controlled rocking and energy dissipating fuses. *Technical Report 174*, John A. Blume Earthquake Engineering Center, Stanford, CA, USA.

[4] Wiebe L, Christopoulos C, Tremblay R, Leclerc M (2013): Mechanisms to limit higher mode effects in a controlled rocking steel frame 2: Large-amplitude shake table testing. *Earthquake Engng Struct. Dyn.*, **42**(7), 1069-1086.

[5] Wiebe L, Christopoulos C (2014): Performance-based seismic design of controlled rocking steel braced frames. II: Design of capacity protected elements. *J. Struct. Eng.*, **141**(9), 04014227 1-10.

[6] Wiebe L, Christopoulos C (2014): Performance-based seismic design of controlled rocking steel braced frames. I: Methodological framework and design of base rocking joint. *J. Struct. Eng.*, **141**(9), 04014226 1-10.

[7] Christopoulos C, Filiatrault A, Folz B (2002): Seismic response of self-centering hysteretic SDOF systems. *Earthquake Engng Struct. Dyn.*, **1**(5), 1131-1150.

[8] Seo C-Y, Sause R (2005): Ductility demands on self-centering systems under earthquake loading. *ACI Structural Journal*, **102**(2), 275-285.

[9] Zhang C, Wiebe L (2015): Parametric study of displacement in self-centering SDOF systems. *Proc. of the 11th Canadian Conf. on Earthquake Engng*, Victoria, BC, Canada.

[10] Rahgozar N, Moghadam A, Aziminejad A (2016): Quantification of seismic performance factors for self-centering controlled rocking special concentrically braced frame. *Struct. Design Tall Spec. Build.*, doi: 10.1002/tal.1279.

[11] American Society of Civil Engineers (ASCE) (2010): Minimum design loads for buildings and other structures. *ASCE/SEI Standard 7-10*, American Society of Civil Engineers, Reston, VA, USA.

[12] Eatherton MR, Ma X, Krawinkler H, Mar D, Billington S, Hajjar J, Deierlein G (2014): Design concepts for controlled rocking of self-centering steel-braced frames. *J. Struct. Eng.*, **140**(11), 4014082 1-10.

[13] Steele TC, Wiebe LDA (2016): Dynamic and equivalent static procedures for capacity design of controlled rocking steel braced frames. *Earthquake Engng Struct. Dyn*., doi: 10.1002/eqe.2765.

[14] Computers and Structures Inc. (CSI) (2015): Extended Three-Dimensional Analysis of Building Structures (ETABS), Ultimate Edition [version 15.0.0]. Computers and Structures Inc., Berkeley, California, USA.

[15] Pacific Earthquake Engineering Research Center (PEER) (2015): Open System for Earthquake Engineering Simulation (OpenSees) [version 2.4.5]. Pacific Earthquake Engineering Research Center, Berkeley, California, USA.

[16] DYWIDAG Systems International Inc. (DSI) (2006): DYWIDAG post-tensioning systems. *Product Brochure*. DYWIDAG Systems International.

[17] Computers and Structures Ins. (CSI) (2007): Perform 3D user's manual. Computers and Structures Inc., Berkeley, California, USA.

[18] Jehel P, Léger P, Ibrahimbegovic A (2014): Initial versus tangent stiffness-based Rayleigh damping in inelastic time history seismic analyses. *Earthquake Engng Struct. Dyn.*, **43**(3), 467-484.

[19] Applied Technology Council (ATC). (2009): Quantification of building seismic performance factors, *FEMA Report P695*, Federal Emergency Management Agency, Washington, D.C., USA.

[20] Vamvatsikos D, Cornell C (2002): Incremental dynamic analysis. *Earthquake Engng Struct. Dyn.*, **31**(3), 491-514.

[21] Baker J (2015): Efficient analytical fragility function fitting using dynamic structural analysis. *Earthquake Spectra*, **31**(1), 579-599.

[22] Baker J, Cornell C (2006): Spectral shape, epsilon and record selection. *Earthquake Engng Struct. Dyn.*, **35**(9),1077-1095.

[23] Haselton C, Baker J, Liel A, Deierlein G (2011): Accounting for ground-motion spectral shape characteristics in structural collapse assessment through an adjustment for epsilon. *J. Struct. Eng.*, **137**(3), 332-344.